Magnitude and size scaling of intervalley coupling in semiconductor alloys and superlattices

Lin-Wang Wang and Alex Zunger
National Renewable Energy Laboratory, Golden, Colorado 80401
(Received 14 July 1997)

Coupling between different Γ, X, and L band-structure valleys is responsible for (a) level anticrossing in superlattices as a function of period, pressure, and electric field and for (b) ''optical bowing'' of band gaps in random alloys. We investigate the symmetry, magnitude, and size scaling of intervalley coupling in semiconductor superlattices and alloys by direct supercell calculations, performed with screened pseudopotentials and a plane-wave basis, considering up to 10^6 atoms/supercell. Projecting the calculated electronic wave functions ψ_i of alloys or superlattices onto the bulk states of the constituent zinc-blende materials shows that ψ_i contain a ''majority representation'' from one or more zinc-blende states γ. The intervalley coupling $E(i,j)$ between the alloy states ψ_i and ψ_j then includes a term $2F(\gamma,\gamma')V(\gamma,\gamma')$ due to the ''majority representations'' γ and γ' of ψ_i and ψ_j, respectively, plus residual terms due to the minority representations. We find the following: (i) In *alloys*, the orbital overlap function $F(\gamma,\gamma')$ is large, since the wave functions are extended. The intervalley coupling element $V(\gamma,\gamma')$ exhibits simple selection rules: being zero for (Γ_{1c},X_{1c}), (Γ_{1c},L_{3c}), (X^x_{1c},X^y_{1c}), etc. (''weak coupling''), and nonzero for (Γ_{1c},X_{3c}), (Γ_{1c},L_{1c}), (L_{3c},X_{1c}), etc. (''strong coupling''). This explains why the Γ-like conduction band of mixed-cation alloys contains zinc-blende Γ_{1c} and L_{1c} character, but not X_{1c}. In the case of strong coupling, $E(i,j)$ scales as $1/\sqrt{\Omega}$, where Ω is the volume, while in the weak-coupling case the entire coupling originates from the ''minority representation,'' and is 20–100 times smaller. The minority representation, however, contributes to the bowing of the band gap vs composition. (ii) In *superlattices*, although the above selection rule for $V(\gamma,\gamma')$ still exists, the magnitude of the intervalley coupling is governed by the overlap function $F(\gamma,\gamma')$. For simple superlattices, $F(\gamma,\gamma')$ is small, since the wave functions are localized in particular segments (''weak coupling''). Consequently, the ''majority representation'' contributes 5–100 times less than in the analogous case of alloys. Furthermore, $E(i,j)$ scales as $1/n^3$, where n is the superlattice period. [S0163-1829(97)05744-5]

I. INTRODUCTION

When an electronic state of a composite system (e.g., A/B heterostructure, A/B nanostructure, or $A_{1-x}B_x$ alloy) consists of bulk Bloch states originating from *a few* band structure valleys (Γ,X,L) of the constituent solids A and B, we say that the system exhibits ''intervalley coupling.'' There are two types of manifestations of intervalley couplings:

In the first type, two states of the composite system are composed each from a different band structure valley of the parent bulk system. When an external field (e.g, pressure,[1–3] alloy composition,[4,5] electric[6] and magnetic fields[7]) is scanned, the energies of the two states of the composite system will anticross due to the mixing (coupling) between them. Figure 1 illustrates this case by depicting (see the inset) the calculated dependence of two conduction-band energy levels $\bar{\Gamma}_1(\Gamma_{1c})$ and $\bar{\Gamma}_1(X_{1c})$ of the $(GaAs)_n/(AlAs)_n$ (001) superlattice on the external pressure. The states have the same $\bar{\Gamma}_1$ symmetry in the superlattice, yet they are derived from distinct valleys (Γ_{1c} and X_{1c}, respectively) of the zinc-blende constituents. The anticrossing gap $E(\Gamma,X)$ (the point of closest approach) can be calculated or measured, thus providing the magnitude of the Γ_{1c}-X_{1c} intervalley coupling in the superlattice. Figure 1 shows how the magnitude of the Γ_{1c}-X_{1c} anticrossing gap oscillates with the superlattice period n, and illustrates how the coupling Γ_{1c}-X_{3c} with a different state X_{3c} oscillates with a different phase. These behaviors will be analyzed below.

In the second type of manifestation of intervalley coupling, a state of the composite system is dominated by contributions from a single valley (e.g., Γ) in the constituent solids. Here the intervalley coupling is demonstrated by the existence of minority contributions from *other* valley minima (e.g., L) in the same state of the composite system. This is shown in Fig. 2(a) for the Γ-like conduction-band minimum (CBM) of the $Ga_{0.7}Al_{0.3}As$ alloy. Its wave function $\psi^{(i)}(\mathbf{r})$

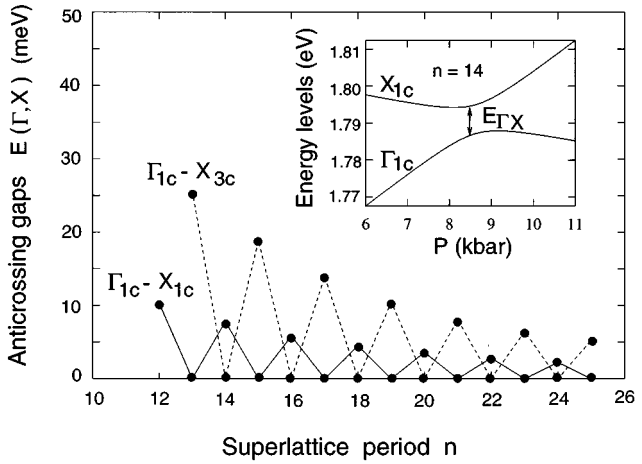

FIG. 1. Magnitudes of $E(\Gamma,X)$ anticrossing gap as functions of superlattice period n in $(GaAs)_n/(AlAs)_n$ (001) superlattices. The inset shows the change of the energy levels as a function of external pressure for $n=14$.

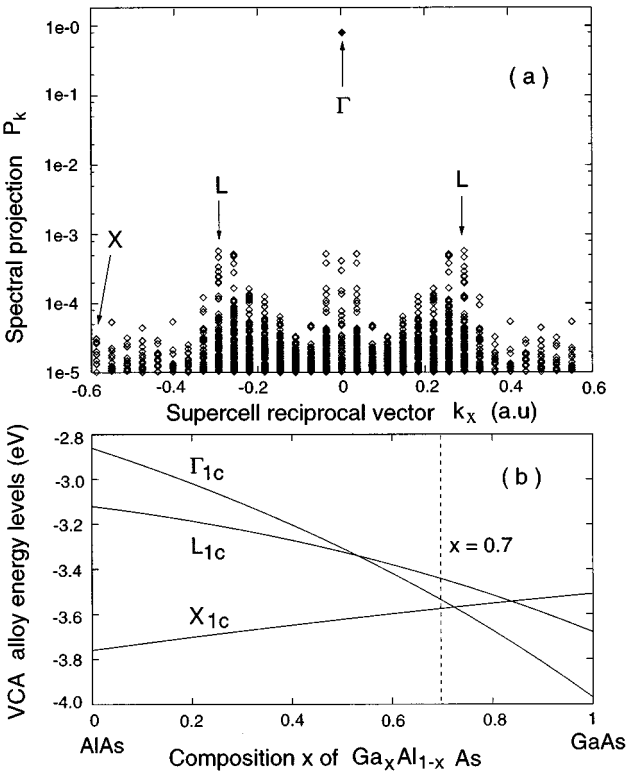

FIG. 2. (a) Spectral analysis [Eq. (1)] of the $\bar{\Gamma}$-like CBM wave function of a 327 680-atom supercell representing the random $Ga_{0.7}Al_{0.3}As$ alloy. The spectrum $P^{\rm CBM}_{(k_x,k_y,k_z)}=\Sigma_m|A^{\rm CBM}_{m,(k_x,k_y,k_z)}|^2$ is plotted as a function of k_x. Each diamond symbol represents one (k_x,k_y,k_z) point. The value of $P^{\rm CBM}_k$ at the Γ point is 0.9136, and the sum of all points equals 1. (b) The VCA alloy energies for different compositions x. The vertical dashed line corresponds to $x=0.7$ for $Ga_{0.7}Al_{0.3}As$.

was calculated via a plane-wave screened pseudopotential method using a $\sim$33 000 atom cubic supercell (see Sec. III). It is then projected onto a set of virtual-crystal-approximation (VCA) zinc-blende Bloch functions $\phi^{\rm VCA}_{m,k}(r)$:

$$\psi^{(i)}(r)=\sum_{m,k} A^{(i)}_{m,k}\phi^{\rm VCA}_{m,k}(r), \tag{1}$$

where k is the reciprocal vector of the supercell within the zinc-blende Brillouin zone and m is the band index. The amplitude $P^{\rm CBM}_k=\Sigma_m|A^{\rm CBM}_{m,k}|^2$ is shown in Fig. 2(a) vs the k points of the supercell. As we can see, a single zinc-blende component $k=\Gamma$ contributes 90% of the total weight of the alloy CBM wave function. Further analysis shows that the weight on $k=\Gamma$ comes mainly from a single zinc-blende VCA state Γ_{1c}. The 10% minority contribution of other k points [mostly from the L point in Fig. 2(a)] results from intervalley coupling. Although small, these minority $\{P^{\rm CBM}_k\}$ components contribute significantly to the optical bowing (a nonlinear dependence of the alloy eigenvalues on composition) in this system.[8,9]

We are interested here in establishing (i) the existence or absence of intervalley coupling $E(\gamma,\gamma')$ between given states γ and γ', (ii) the magnitude of the coupling, and (iii) its scaling with the systems size. Regarding item (i), i.e., the *existence or absence* of intervalley coupling, this is often discussed in the literature by considering the overall symmetry of the composite system.[10,11] This type of analysis can be used, for example, to explain[10] why the Γ_{1c}-X_{1c} anticrossing gap is zero for odd n (Fig. 1), while the anticrossing gap for Γ_{1c}-X_{3c} is zero for even n. But the applicability of the symmetry-based analysis is limited to highly symmetric composite systems. In many cases, such as the alloy system illustrated in Fig. 2(a), the overall symmetry is too low to be useful in this respect. Regarding (ii), the *magnitude and scaling* of intervalley coupling is important for understanding optical bowing in alloys,[8,9] the indirect optical transition without phonon interaction,[1,12] the resonant intervalley tunneling in quantum well electron transmission,[13] and the characteristic pressure-induced changes of photoluminescence.[14,2] Regarding (iii), the size scaling of $E(\gamma,\gamma')$ is related to the order of the transition from direct to indirect gaps. If $E(\Gamma,X)\to 0$, for infinite alloy supercells, then the $\Gamma\to X$ transition in $Al_xGa_{1-x}As$ as x changes is first order.[4] Otherwise, it is second order.

Here we will analyze the magnitudes and scalings of intervalley couplings for alloys and superlattices. We find that the magnitude of intervalley coupling comes from a ''majority contribution'' and a ''minority contribution.'' In the case of alloys, whether or not the majority contribution is zero is determined by a selection rule we derived [Eq. (10) below]. When the majority contribution is not zero, the magnitude of the intervalley coupling is 20–100 times larger than the cases where the majority contribution is zero and the intervalley coupling scales as $1/\sqrt{\Omega}$, where Ω is the volume of supercell. In the cases of simple superlattices, we find that the majority contribution is always small, due to a vanishing overlap function [Eq. (7) below]. In these cases, the intervalley coupling comes from the minority contribution terms, and it scales as $1/n$, where n is the period of the superlattice.

II. MAJORITY AND MINORITY CONTRIBUTIONS TO INTERVALLEY COUPLING

It is useful to define a ''majority representation'' for a given eigenstate of the composite system using the spectral expansion of Eq. (1). As shown in Fig. 2(a) (computational details will be given in Sec. III), a single zinc-blende wave vector ($k=\Gamma$, and in fact a single zinc-blende state Γ_{1c}) contributes more than 90% of the total weight to the alloy $\bar{\Gamma}$-type CBM. This Γ_{1c} constituent state will thus be referred as the ''majority representation'' of the $\bar{\Gamma}$ alloy state. A similar analysis of the $\bar{\Gamma}$-type CBM of the $(GaAs)_{96}/(AlAs)_{96}$ superlattice at zero pressure is shown in Fig. 3. We see that although the spectral function $P^{\rm CBM}_k=\Sigma_m|A^{\rm CBM}_{m,k}|^2$ peaks at the zinc-blende wave vector $k=0$, the single zinc-blende state (Γ_{1c}) accounts for only 43% of the total spectral weight. Including the three k points around Γ (enclosed box in Fig. 3) accounts for 93% of the total weight, whereas inclusion of five k points accounts for 99.6% of the total. To elaborate on this discussion, we separate the right-hand side of Eq. (1) into two terms:

$$\psi^{(i)}(r)=\sum_{\delta k} A^{(i)}_{n_0,k_0+\delta k}\phi^{\rm VCA}_{n_0,k_0+\delta k}+\sum_{n,k}{}' A^{(i)}_{n,k}\phi^{\rm VCA}_{n,k}(r). \tag{2}$$

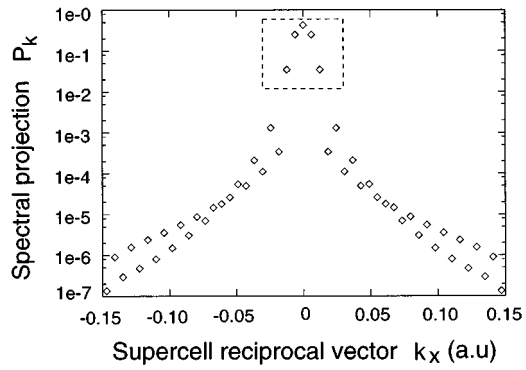

FIG. 3. The spectral analysis [Eq. (1)] of the $\bar{\Gamma}$-like CBM state of a $(GaAs)_{96}/(AlAs)_{96}$ (001) superlattice. $P^{\mathrm{CBM}}_{(k_x,k_y,k_z)} = \Sigma_m |A^{\mathrm{CBM}}_{m,(k_x,k_y,k_z)}|^2$ is plotted as a function of k_x, and $k_y = k_z = 0$ for this supercell. The P_k value at the Γ point is 0.43.

The first term is limited to the neighborhood δk of k_0 and gives the ''majority representation.'' δk equals zero for alloys (Fig. 2), but includes a few points for superlattices (Fig. 3). We will use $\gamma=(n_0,k_0)$ to denote the constituent basis function at the center of the majority representation.

The anticrossing gap $E(\gamma,\gamma')$ between the states $\psi^{(i)}$ [with a majority contribution $\gamma=(n_0,k_0)$] and $\psi^{(j)}$ [with a majority contribution $\gamma'=(n_0',k_0')$] is

$$E(\gamma,\gamma') = 2\langle \psi^{(i)}|V(\mathbf{r})|\psi^{(j)}\rangle = 2\sum_{\delta k,\delta k'} A^{(i)*}_{n_0,k_0+\delta k} A^{(j)}_{n_0',k_0'+\delta k'} \times \langle \phi^{\mathrm{VCA}}_{n_0,k_0+\delta k}|V(\mathbf{r})|\phi^{\mathrm{VCA}}_{n_0',k_0'+\delta k'}\rangle + \sum_{n,n',k,k'}{}' R(n,n',k,k'), \tag{3}$$

where $V(\mathbf{r})$ is the total potential of the composite system, and the sums over k and k' are centered around k_0 and k_0' ($k_0' \neq k_0$), respectively, with noncommon domains. In Eq. (3), the first term comes from the majority representation term in Eq. (2), while $R(n,n',k,k')$ includes the residuals.

We will first discuss ways to estimate the magnitude of the first term in Eq. (3) under a simplified but common assumption about the potential $V(\mathbf{r})$ (we will discuss the possible errors of this assumption in Sec. VI): We will assume that the effective potential is given by a linear superposition of overlapping (but not necessarily spherical) atomic potentials $\Delta V_{AB}(\mathbf{r})$ on ideal, unrelaxed lattice sites $\mathbf{R}^0$. We consider a composite system made of a zinc-blende lattice with N_A A atoms, N_B B atoms (both cation) and $N_A+N_B=N$ anions C. Using $V(\mathbf{r};N_A,N_B)$ to denote the total potential of this system, we consider the form

$$V(\mathbf{r};N_A,N_B) = V(\mathbf{r};0,N) + \sum_{\mathbf{R_A^0}} \Delta V_{AB}(\mathbf{r}-\mathbf{R_A^0}), \tag{4}$$

where $V(\mathbf{r},0,N)$ is the total potential of the pure BC crystal, and $\mathbf{R_A^0}$ is the ideal (unrelaxed) cation atomic position of atom A. $\Delta V_{AB}(\mathbf{r})$ is the change in potential due to a substituation of one B atom with one A atom. $\Delta V_{AB}(\mathbf{r})$ is assumed to be independent of the local environment around $\mathbf{R_A^0}$. Under this assumption, $\Delta V_{AB}(\mathbf{r})$ must have T_d symmetry around its origin. This is clear that if we set $N_A=1$, then $\Delta V_{AB}(\mathbf{r}) = V(\mathbf{r};1,N-1) - V(\mathbf{r};0,N)$, which has T_d symmetry. Equation (4) is satisfied, e.g., by common empirical pseudopotential[15–17] or other non-self-consistent potential schemes when there is no atomic relaxations.

Substituting Eq. (4) into Eq. (3) gives an anticrossing gap

$$E(\gamma,\gamma') = 2\langle \psi^{(i)}|V|\psi^{(j)}\rangle = 2F(\gamma,\gamma')V(\gamma,\gamma') + 2\sum_{n,n',k,k'}{}' R'(n,n',k,k'). \tag{5}$$

Here

$$F(\gamma,\gamma') = \sum_{\delta k,\delta k'} A^{(i)*}_{n_0,k_0+\delta k} A^{(j)}_{n_0',k_0'+\delta k'} S(k_0-k_0'+\delta k-\delta k') \tag{6}$$

is an envelope overlap function, and

$$S(\mathbf{k}) = \frac{1}{N}\sum_{\mathbf{R_A^0}} e^{i\mathbf{k}\cdot\mathbf{R_A^0}} \tag{7}$$

is a structure factor, while the VCA intervalley coupling element is

$$V(\gamma,\gamma') = N\langle \phi^{\mathrm{VCA}}_{\gamma}|\Delta V_{AB}(\mathbf{r})|\phi^{\mathrm{VCA}}_{\gamma'}\rangle. \tag{8}$$

Also note that, if we use ϕ^{VCA}_{γ}, $\phi^{VCA}_{\gamma'}$ to replace $\psi^{(i)}$ and $\psi^{(j)}$ in Eq. (5), we have a single-k-point (SKP) anticrossing gap,

$$E_{\mathrm{SKP}}(\gamma,\gamma') = 2\langle \phi^{\mathrm{VCA}}_{\gamma}|V(\mathbf{r})|\phi^{\mathrm{VCA}}_{\gamma'}\rangle = 2S(k_0-k_0')V(\gamma,\gamma'). \tag{9}$$

We have introduced the quantity N into Eqs. (7) and (8), which is the total number of primary cells in the system, to ensure that $V(\gamma,\gamma')$ is an intensive quantity (independent of the system size). The $R'(n,n',k,k')$ term in Eq. (5) contains the residuals R of Eq. (3), and additional residual terms which are produced when we replace $\phi^{\mathrm{VCA}}_{n_0,k_0+\delta k}$ with $\phi^{\mathrm{VCA}}_{n_0,k_0}$ in the evaluation of Eq. (8) in the cases of superlattices. We will call the first term in Eq. (5) the majority contribution to the intervalley coupling, while the residual term R' in Eq. (5) the minority contribution.

From the above definitions we can now derive the central result of this section. We define our X_{1c} and X_{3c} states by choosing the origin of the point group operation at the anion site. As a result, in the systems we studied here, the lowest conduction band state at X point is the X_{1c} (anion S+cation P) and the next lowest state is the X_{3c} (cation S+anion P). For mixed-cation alloys, we find that $V(\gamma,\gamma')$ of the following pairs are exactly zero for the potential of Eq. (4):

$$V(\Gamma_{1c},X_{1c}) = V(\Gamma_{1c},L_{3c}) = V(X^x_{1c},X^y_{1c}) = V(X^x_{1c},X^y_{3c}) = 0. \tag{10}$$

[For $V(X^x_{1c},X^y_{1c})$ and $V(X^x_{1c},X^y_{3c})$, (x,y) can be replaced by (x,z) or (y,z)]. For mixed-anion alloys, we need to exchange X_{1c} with X_{3c} in Eq. (10). These selection rules can be derived by considering the symmetries of $\phi^{\mathrm{VCA}}_{\gamma}$ and the T_d symmetry of $\Delta V_{AB}(\mathbf{r})$ in Eq. (8). We see that for superposition-type potentials without lattice relaxation, the

entire intervalley coupling between the states of Eq. (10) originates from the minority representation of the wave functions. On the other hand, for other pairs of states, we have a nonzero majority contribution to the coupling [provided that the overlap factor $F(\gamma,\gamma')$ is not zero].

In the remainder of this paper, we will show that we can distinguish two main types of intervalley couplings:

(i) *Large majority contribution in alloy (''strong coupling''):* This is the coupling between the ''VCA-allowed pairs'' [e.g., Γ_{1c}-X_{3c}, Γ_{1c}-L_{1c}, X_{1c}-L_{1c}, X_{1c}-L_{3c}, and X^x_{3c}-X^y_{3c} which are not in Eq. (10)]. We will see that, in alloys, where the coupling states are extended and have a large overlap $F(\gamma,\gamma')$, the majority term alone, using the model potential, can explain the full coupling quantitatively. The full coupling will be calculated by a direct diagonalization technique (see Sec. III), while the model coupling will be represented by the leading terms of Eqs. (5)–(10). Evaluating the structure factor $S(k_0-k_0')$ using the random distribution of A atoms in Eq. (7), we have

$$E^{\rm alloy}_{\rm maj}(\gamma,\gamma')=2F(\gamma,\gamma')V(\gamma,\gamma')\cong 2S(k_0-k_0')V(\gamma,\gamma') = \sqrt{\frac{8x(1-x)}{N}}\,V(\gamma,\gamma'), \tag{11}$$

which scales as $1/\sqrt{\Omega}$, where $\Omega\propto N$ is the volume of the system and x is the alloy composition of constituent A. Note that, for an alloy, this majority contribution term coincides with the single-k-point anticrossing gap of Eq. (9). We will see later that this is no longer true for superlattices.

(ii) *Small majority contribution (''weak coupling''):* There are two cases where this happens: (a) Couplings between the ''VCA-forbidden'' states of Eq. (10) in an alloy system. In this case, the majority contribution is exactly zero, and the entire coupling comes from the minority contribution. We found that in these cases the magnitude of the coupling is 20–100 times smaller than in the strong-coupling case. (b) Intervalley couplings in simple superlattices. The majority contributions of these couplings are always small due to a vanishing overlap factor $F(\gamma,\gamma')$ stemming from the localization of the wave functions. The magnitude of the coupling scales as $1/n^3$, where n is the period of the superlattice.

III. DIRECT CALCULATIONS OF THE INTERVALLEY COUPLINGS

To examine the different models of intervalley coupling, we need benchmark accurate calculations. To do so, we solve the single-particle Schrödinger equation

$$[-\tfrac{1}{2}\nabla^2+V(\mathbf{r};N_A,N_B)]\psi^{(i)}(\mathbf{r})=\epsilon_i\psi^{(i)}(\mathbf{r}), \tag{12}$$

using a superposition of atomic screened pseudopotentials:[16]

$$V(\mathbf{r};N_A,N_B)=\sum_{\alpha=A,B,C}\sum_{\mathbf{R}_\alpha} v_\alpha(|\mathbf{r}-\mathbf{R}_\alpha|). \tag{13}$$

Here $v_\alpha(r)$ is the screened pseudopotential fitted[17] to bulk band structures and band offsets. Previous calculations using the same empirical pseudopotentials model (EPM) yield superlattice Γ-X couplings close to experimental values.[18] The alloy optical bowing parameters calculated using these empirical pseudopotentials also agree well with experimental results.[19,20] For bulk AC and BC crystals, the wave functions are close to self-consistent local-density approximation [21,17] results.

We use two methods to solve the single-particle Schrödinger equation (12): For systems containing up to 30 000 atoms, we have used the ''folded spectrum method'' (FSM).[22] Instead of solving the original Hamiltonian $\hat{H}$, this method solves the folded Hamiltonian $(\hat{H}-\epsilon_{\rm ref})^2$, where $\epsilon_{\rm ref}$ is a reference energy placed inside the band gap. The computational effort of this method scales linearly to the size of the system. For systems containing more than 30 000 (and up to a few million) atoms, the folded spectrum method becomes too expensive to use. For these cases, we have used a ''linear combination of bulk bands'' (LCBB) method.[18] This method expands the system eigenstate wave functions by the constituent bulk Bloch wave functions at many k points. By selecting the physically important basis functions, we can diagonalize a million-atom system by using a few thousand basis functions. The resulting eigenvalues have errors of just a few meV with respect to a full basis (e.g., the FSM) approach. The intervalley coupling amplitudes obtained with the LCBB method are very close to the ''exact'' results obtained with the folded spectrum method for systems where both methods can be applied.

Being able to calculate the eigenstates and eigenvalues of a given system, the intervalley coupling is obtained by performing a few calculations of Eq. (12) at different pressures. The anticrossing curves shown in the inset of Fig. 1 are obtained and the anticrossing gap $E(\gamma,\gamma')$ is measured directly from the curves. The wavefunctions can also be projected to the VCA basis to obtain the spectral analysis shown in Figs. 2 and 3.

IV. INTERVALLEY COUPLINGS IN ALLOYS: STRONG OR WEAK COUPLINGS ACCORDING TO SELECTION RULE

A. Size scaling

Figure 4 shows the magnitudes of the *directly calculated* Γ_{1c}-X_{1c} and Γ_{1c}-X_{3c} anticrossing gaps (symbols) for the $Ga_{0.5}Al_{0.5}As$ alloys as a function of the supercell size, ranging from $N=10^4$–10^6 atoms. We assume unrelaxed atomic sites and a superposition potential. We see that, as pointed out by Koiller and Capaz,[4] the Γ-X coupling $E(\gamma,\gamma')$ approaches zero for an infinitely large alloy supercell. This implies that the optical transition changes abruptly from a direct transition to an indirect transition when the Γ and X states cross each other.[4,23] For finite supercells, $E(\gamma,\gamma')$ is not zero, and thus can be measured experimentally from the optical transition. The finite supercell size of the alloy can be realized by the confinement of the wave functions, either due to natural composition fluctuation in ideal alloys,[24] or through controlled growth of alloy quantum dots.[25] The magnitude of $E(\gamma,\gamma')$ can also be estimated from our model: the solid line in Fig. 4 shows the predicted curve for the configuration averaged magnitude of the Γ_{1c}-X_{3c} coupling by considering only the majority contribution term [Eq. (11)].

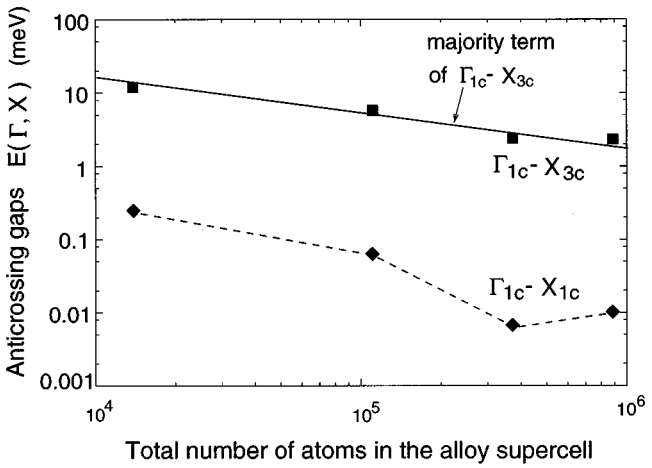

FIG. 4. The directly calculated anticrossing gaps $E(\Gamma_{1c},X_{1c})$ and $E(\Gamma_{1c},X_{3c})$ (symbols) for random $Ga_{0.5}Al_{0.5}As$ alloys at different supercell sizes. The solid line is the majority contribution of the $E(\Gamma_{1c},X_{3c})$ from Eq. (11) [with $V(\Gamma_{1c},X_{3c})=0.374$ eV for the pseudopotentials used here]. The dashed line is drawn to guide the eye.

We use $V(\Gamma_{1c},X_{3c})=0.374$ eV, obtained from our wavefunctions. This gives (for $x=0.5$ alloy composition) $E_{\rm maj}^{\rm alloy}(\Gamma_{1c},X_{3c})=1.06/\sqrt{N}$ eV, which agrees well with the directly calculated values (Fig. 4), demonstrating that in this case, the contribution of the minority representation (included in the direct calculation, but omitted in the model calculation) is small.

B. Why is Γ_{1c}-X_{3c} coupling stronger than Γ_{1c}-X_{1c}

It is clear from Fig. 4 that the Γ_{1c}-X_{3c} anticrossing gap (''strong coupling'') is 20–100 times larger than the Γ_{1c}-X_{1c} results (''weak coupling''). This can be explained by the fact that the majority contribution of the Γ_{1c}-X_{1c} coupling in Eq. (5) is zero according to Eq. (10), while, for Γ_{1c}-X_{3c} coupling, it is not zero.

C. L_{1c} minority representation

Figure 2(a) shows that the largest *minority* representation to the $Ga_{0.7}Al_{0.3}As$ alloy comes from L, not X. This is surprising since at this composition the energy level of X_{1c} are closer to Γ_{1c} than the level of L_{1c} [Fig. 2(b)]. This phenomenon can be explained using perturbation theory. When the majority representation has a large coefficient, the spectral expansion formula in Eq. (2) can be further simplified as

$$\psi^{alloy}(\mathbf{r})\cong A_\gamma\phi_\gamma^{\rm VCA}+\sum_{(n,k)\neq\gamma}A_{n,k}\phi_{n,k}^{\rm VCA}. \tag{14}$$

The minority amplitudes $A_{n,k}$ can be obtained approximately using first-order perturbation theory,

$$A_{n,k}\approx\frac{\langle\phi_\gamma^{\rm VCA}|V|\phi_{n,k}^{\rm VCA}\rangle}{\epsilon_{n,k}^{\rm VCA}-\epsilon_\gamma^{\rm VCA}}. \tag{15}$$

We see that the minority representation $A_{n,k}$ is directly proportional to $\langle\phi_\gamma^{\rm VCA}|V|\phi_{n,k}^{\rm VCA}\rangle=F(\gamma,\gamma')V(\gamma,\gamma')$, which is the majority contribution term to the anticrossing gap in Eq. (11). We can now see that the spectral density $P_k=\Sigma_m|A_{m,k}|^2$ is small around $k=X$. First, X_{3c} couples only weakly into the alloy CBM, since $\epsilon^{\rm VCA}(X_{3c})$ is far above $\epsilon^{\rm VCA}(\Gamma_{1c})$, so the energy denominator in Eq. (15) is large. As a result, we can ignore the contribution of X_{3c} state in Eq. (14). Furthermore, according to Eq. (10), $\langle\phi_{\Gamma_{1c}}^{\rm VCA}|V|\phi_{X_{1c}}^{\rm VCA}\rangle$ is exactly zero. Thus the corresponding $A_{n,k}$ for X_{1c} should also be very small (nonzero value comes only from second-order perturbation effects). Thus $P_k=\Sigma_m|A_{m,k}|^2$ is small around X. On the other hand, P_k around L is much larger and forms a peak, because the corresponding coupling is not required to be zero by Eq. (10). Using $V(\Gamma_{1c},L_{1c})=0.467$ eV calculated from our EPM potential, and $\epsilon_{L_{1c}}^{\rm VCA}-\epsilon_{\Gamma_{1c}}^{\rm VCA}=0.091$ eV from Fig. 2(b), from Eqs. (11) and (15) we obtain that $A_{L_{1c}}^2=0.67\times10^{-3}$, which is close to the directly calculated result of 0.57×10^{-3}, as shown in Fig. 2(a). Thus, in the cation-mixed alloys, the Γ-like CBM has a majority representation originating from zinc blende Γ_{1c}, and a minority representation originating from L_{1c}.

D. Effect of intervalley coupling on alloy optical bowing

The existence of minority $A_{n,k}$ terms for $(n,k)\neq\gamma$ in Eq. (14) contributes significantly to the bowing of the alloy valence-band maximum (VBM) and CBM states. The bowing coefficient $b_{\rm tot}$ is defined in the following description of the alloy energy:

$$E(x)=E_0+ax-b_{\rm tot}x(1-x), \tag{16}$$

where x is the alloy composition and E_0 is the energy for one constituent crystal corresponding to $x=0$. The bowing coefficient $b_{\rm tot}$ can be divided into contributions from VCA states (intrinsic bowing) and contributions from intervalley coupling[8] (repulsion effect): $b_{\rm tot}=b_{\rm VCA}+b_{\rm coupl}$. The intervalley coupling effect can be expressed as a second-order perturbation term[9] [$b_{\rm coupl}=\Delta E_\gamma/x(1-x)$]:

$$\Delta E_\gamma=x(1-x)\frac{1}{N}\sum_{nk}\frac{|V(r,nk)|^2}{\epsilon_\gamma-\epsilon_{nk}}, \tag{17}$$

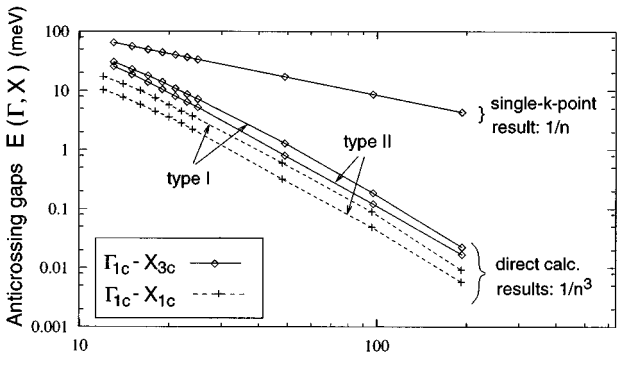

FIG. 5. The anticrossing gaps $E(\Gamma_{1c},X_{1c})$ and $E(\Gamma_{1c},X_{3c})$ for $(GaAs)_n/(AlAs)_n$ superlattices of different periods n, using different empirical pseudopotentials. The type-II EPM results correspond to real physical situations for GaAs/AlAs systems. The upper curve is the single-k-point prediction of Eq. (9).

TABLE I. Magnitudes of single-k-point intervalley coupling (in meV) $\langle \phi_\gamma^{\rm VCA}|V(\mathbf{r})|\phi_{\gamma'}^{\rm VCA}\rangle$ evaluated using VCA wave functions. The potential $V(\mathbf{r})$ is obtained using a cubic supercell containing 64 atoms. The values in the upper half of the table are predicted to be zero by superposition assumption Eq. (4), under which $\langle \phi_\gamma^{\rm VCA}|V(\mathbf{r})|\phi_{\gamma'}^{\rm VCA}\rangle = S(\mathbf{k_0}-\mathbf{k_0'})V(\gamma,\gamma')$ [Eq. (9)]. RMS stands for root mean square values. ''NZ'' in the last column stands for ''not zero.''

$\gamma-\gamma'$	$\langle\phi_\gamma\|V\|\phi_{\gamma'}\rangle$ $Ga_{0.5}Al_{0.5}As$ LDA (unrelaxed)	$\langle\phi_\gamma\|V\|\phi_{\gamma'}\rangle$ $In_{0.5}Ga_{0.5}As$ EPM (unrelaxed)	$\langle\phi_\gamma\|V\|\phi_{\gamma'}\rangle$ $In_{0.5}Ga_{0.5}As$ EPM (relaxed)	S	$\langle\phi_\gamma\|\Delta v\|\phi_{\gamma'}\rangle$ $V(\gamma,\gamma')$
$\Gamma_{1c}-X_{1c}^x$	0.046	0	−4.55	$\frac{4}{32}$	0
$\Gamma_{1c}-X_{1c}^y$	0.027	0	7.46	$\frac{12}{32}$	0
$\Gamma_{1c}-X_{1c}^z$	−0.042	0	−2.84	0	0
$X_{1c}^x-X_{1c}^y$	−0.020	0	−3.49	0	0
$X_{1c}^x-X_{1c}^z$	−0.147	0	9.06	$\frac{12}{32}$	0
$X_{1c}^y-X_{1c}^z$	−0.008	0	−4.74	$\frac{4}{32}$	0
$\Gamma_{1c}-L_{3c}^{(111)}(1)$	−0.004	0	−3.11	$\frac{8}{32}$	0
$\Gamma_{1c}-L_{3c}^{(111)}(2)$	0.029	0	−3.07	$\frac{8}{32}$	0
$X_{1c}^x-X_{3c}^y$	0.004	0	−1.07	0	0
$X_{1c}^y-X_{3c}^x$	0.003	0	−0.75	0	0
$\Gamma_{1c}-X_{3c}^z$	−0.01	0	0.79	0	NZ
$X_{3c}^x-X_{3c}^y$	−0.04	0	1.49	0	NZ
$L_{1c}^{(111)}-X_{1c}^z$	0.24	0	4.91	0	NZ
$L_{1c}^{(111)}-X_{3c}^z$	−0.28	0	−3.64	0	NZ
RMS	0.109	0	4.33		
$\Gamma_{1c}-X_{3c}^x$	38.78	8.65	−10.67	$\frac{4}{32}$	NZ
$\Gamma_{1c}-X_{3c}^y$	116.40	25.96	−32.60	$\frac{12}{32}$	NZ
$X_{3c}^x-X_{3c}^z$	139.70	−36.16	123.30	$\frac{12}{32}$	NZ
$X_{3c}^y-X_{3c}^z$	46.56	−12.05	40.86	$\frac{4}{32}$	NZ
$\Gamma_{1c}-L_{1c}^{(111)}$	−91.18	−38.35	−6.52	$\frac{8}{32}$	NZ
$L_{1c}^{(111)}-L_{1c}^{(1\bar{1}1)}$	149.60	1.19	19.80	$\frac{12}{32}$	NZ
$L_{1c}^{(111)}-X_{1c}^x$	19.70	−18.68	2.18	$\frac{4}{32}$	NZ
$L_{1c}^{(111)}-X_{1c}^y$	19.48	−18.68	1.21	$\frac{4}{32}$	NZ
$L_{1c}^{(111)}-X_{3c}^x$	−37.45	−10.86	−20.00	$\frac{4}{32}$	NZ
$L_{1c}^{(111)}-X_{3c}^y$	−37.64	−10.86	−26.21	$\frac{4}{32}$	NZ
RMS	84.27	21.46	44.25		

where $V(r,nk)$ is just the $V(\gamma,\gamma')$ of Eq. (8). This second-order perturbation in eigenenergy corresponds to the first-order perturbation in wave function of Eq. (15). If we neglect the intervalley coupling, i.e., if we use only the majority representation state γ as the alloy wave function, we obtain $b_{\rm tot}=b_{\rm VCA}$. In the case of $Ga_xAl_{1-x}As$, we find that $b_{\rm VCA}=-0.38$ eV for the Γ_{1c}-Γ_{15v} energy gap, while the experimental result is $b_{\rm tot}^{\rm expt}=0.37$ eV.[26] This large discrepancy is due to $b_{\rm coupl}=b_{\rm tot}-b_{\rm VCA}$. In our current supercell calculation, $b_{\rm tot}=0.45$ eV,[20] which is close to the experimental result. The large difference $b_{\rm VCA}-b_{\rm tot}$ comes mainly from intervalley couplings in the conduction band. If we separate the band gap $b_{\rm tot}$ into $b_{\rm CBM}-b_{\rm VBM}$, we find that

$$b_{\rm VBM}=-0.05,\quad b_{\rm CBM}=-0.43:\ \text{VCA},$$

$$b_{\rm VBM}=-0.05,\quad b_{\rm CBM}=0.78:\ \text{Coupling},$$

$$b_{\rm VBM}=-0.10,\quad b_{\rm CBM}=0.35:\ \text{Total}. \tag{18}$$

Here $|b_{\rm CBM}(\text{coupl})|\gg|b_{\rm VBM}(\text{coupl})|$; this is because the intervalley coupling is much stronger in the conduction band than in the valence band. Using the selection rule of Eq. (10), we can further analyze that the $b_{\rm CBM}$(coupl) of the alloy Γ_{1c} state is mainly due to minority representation at L_{1c}, instead of minority representation at X_{1c}.

V. INTERVALLEY COUPLINGS IN SUPERLATTICES: WEAK COUPLING DUE TO SMALL OVERLAP FUNCTION $F(\gamma,\gamma')$

A. Why is Γ-X coupling weaker in superlattices than in alloys

In Fig. 1, we see the magnitudes of the anticrossing gaps of the Γ_{1c}-X_{3c} and Γ_{1c}-X_{1c} pairs in (001) $(AlAs)_n/(GaAs)_n$ superlattices. Although in the superlattice the Γ_{1c}-X_{3c} coupling is larger than the Γ_{1c}-X_{1c} coupling, surprisingly the difference is not as large as in the case of the $Ga_{0.5}Al_{0.5}As$ random alloy (Fig. 4), where the ratio was 20–100. To see how much of the Γ_{1c}-X_{3c} coupling comes from the majority

contribution, we compare in Fig. 5 the directly calculated Γ_{1c}-X_{3c} anticrossing gap with the results obtained using the single-k-point coupling of Eq. (9). In the alloy, this single-k-point coupling represented the majority contribution term, and thus agreed well with the directly calculated results (Fig. 4). But in superlattices, the single-k-point result is much larger (5–100 times) than the directly calculated results. Furthermore, while the results of the single-k-point coupling scale in superlattice as $1/n$, where n is the superlattice period, our directly calculated Γ_{1c}-X_{3c} and Γ_{1c}-X_{1c} couplings scale as $1/n^3$. We find that these differences are due to the localization of the superlattice states $\psi^{(i)}$ and $\psi^{(j)}$. As a result, the extended single-k-point VCA states $\phi_\gamma^{\mathrm{VCA}}$ and $\phi_{\gamma'}^{\mathrm{VCA}}$ cannot be used to represent $\psi^{(i)}$ and $\psi^{(j)}$ adequately: Due to the localization of $\psi^{(i)}$ and $\psi^{(j)}$ states, the overlap function $F(\Gamma,X)$ has a small magnitude. $F(\Gamma,X)$ can be estimated using envelope functions of an effective-mass model. If the barrier of the effective-mass model is infinity, $F(\Gamma,X)$ is zero. If the barrier if finite, analytical solutions lead to $F(\Gamma,X)\propto 1/n^3$. This explains the $1/n^3$ scaling in Fig. 5.

B. Effect of type-I/type-II band offsets on coupling

In a GaAs/AlAs system, the conduction-band energies of the constituents have the following alignment: $\epsilon_{\mathrm{GaAs}}(\Gamma_{1c}) < \epsilon_{\mathrm{AlAs}}(\Gamma_{1c})$, $\epsilon_{\mathrm{GaAs}}(X_{1c}) > \epsilon_{\mathrm{AlAs}}(X_{1c})$, and $\epsilon_{\mathrm{GaAs}}(X_{3c}) > \epsilon_{\mathrm{AlAs}}(X_{3c})$. Thus the superlattice state induced from Γ_{1c} is localized in the GaAs region, while the superlattice states induced from X_{1c} and X_{3c} are localized in the AlAs region. This band-level alignment is called ''type-II'' alignment.[27] In type-II systems, the overlap function $F(\Gamma,X)$ has contributions only from the interface, and has $1/n^3$ scaling for large n, which explains the $1/n^3$ scaling of the Γ_{1c}-X_{3c} coupling as shown in Fig. 5. Since the overall interaction between the two localized states is proportional to the overlap between their envelope-function overlaps, the residual term in Eq. (5) also scales as $1/n^3$, which explains why Γ_{1c}-X_{1c} also scales as $1/n^3$.

The above discussions involve intervalley couplings between two states that are localized in different regions (type-II alignment). We would like to know what happens when the Γ and X states are localized in the same region (type-I alignment).[27] To study this, we have deliberately changed the pseudopotential v_α of Eq. (13), so that $\epsilon_{\mathrm{GaAs}}(\Gamma_{1c}) < \epsilon_{\mathrm{AlAs}}(\Gamma_{1c})$, $\epsilon_{\mathrm{GaAs}}(X_{1c}) < \epsilon_{\mathrm{AlAs}}(X_{1c})$, and $\epsilon_{\mathrm{GaAs}}(X_{3c}) < \epsilon_{\mathrm{AlAs}}(X_{3c})$. Thus the Γ_{1c}, X_{1c}, and X_{3c} states are now all localized in the GaAs region. To compare results with the original type-II case, we also fitted $V(\Gamma_{1c},X_{3c}) = 0.401$ eV, close to the original EPM value of 0.374 eV. We ensured that the Ga-Al atomic pseudopotential differences in the reciprocal space are similar to those in the original potentials. The type-I Γ_{1c}-X_{3c} and Γ_{1c}-X_{1c} anticrossing gaps are plotted in Fig. 5. Their values are seen to be larger than the type-II results by a factor of 1.5–2, but they still have the same $1/n^3$ scaling. The value of the Γ_{1c}-X_{3c} anticrossing gap is still much smaller than the single-k-point results. This indicates that the majority contribution of the Γ_{1c}-X_{3c} coupling in Eq. (5) is still much smaller than the single-k-point result. This is again due to the small value of the overlap function $F(\gamma,\gamma')$ ($\propto 1/n^3$), caused by the phase factor $\exp[i(\mathbf{k}_\Gamma-\mathbf{k}_X)\cdot\mathbf{r}]$ in the evaluation of Eq. (6). This again can be proved using the envelope function of an effective-mass model.

In conclusion the majority contribution of the intervalley coupling of one-dimensional (1D) superlattices is always much smaller than the single-k-point result. This is due to the small value of $F(\gamma,\gamma')$, regardless whether the band alignment is type I or II. The resulting superlattice anticrossing gaps scale as $1/n^3$, where n is the period of the superlattice. Although we do not explicitly study quantum wires and quantum dots in this paper, we point out that the above conclusion is also true for 2D quantum wires and 3D quantum dots,[18] where n is the linear dimension (not the area or volume) of the nanostructure.

However, this conclusion is no longer true if there is a δ layer in the superlattice. This is demonstrated by placing one monolayer of AlAs in the middle of GaAs region in the $(\mathrm{GaAs})_{97}/(\mathrm{AlAs})_{97}$ superlattice $[\rightarrow(\mathrm{GaAs})_{48}(\mathrm{AlAs})_1(\mathrm{GaAs})_{48}(\mathrm{AlAs})_{97}]$. Using the type-I EPM, the Γ_{1c}-X_{3c} anticrossing gap increases 100 times, from the original 0.19 meV to 23 meV. This is due to the increase of $F(\gamma,\gamma')$; thus the increase of the majority contribution. On the other hand, the Γ_{1c}-X_{1c} anticrossing is 1.6 meV, much smaller than the Γ_{1c}-X_{3c} result. This is due to the still vanished majority contribution of Γ_{1c}-X_{1c} according to Eq. (10).

VI. NONSUPERPOSITION EFFECTS ON INTERVALLEY COUPLING

Our analytical model involves the use of selection rule Eq. (10). This rule is satisfied under the assumption of a superpositional potential of unrelaxed atoms, i.e., Eq. (4). Here we will test the validity of this approximation, i.e., the effects of self-consistent potential and atomic relaxations on Eq. (4).

A. Effects of self-consistency on superposition assumption

We use the self-consistent local density approximation (LDA) (Ref. 21) to generate potential $V(\mathbf{r};N_A,N_B)$. The self-consistent potential can no longer be written as the sum of the atomic potentials as in Eq. (4). Instead of checking Eq. (4) directly [which might be subjected to the uncertainty of the definition of $\Delta V_{AB}(\mathbf{r}-\mathbf{R_A^0})$], we choose to evaluate the quantity $\langle\phi_\gamma^{\mathrm{VCA}}|V(\mathbf{r})|\phi_{\gamma'}^{\mathrm{VCA}}\rangle = E_{\mathrm{SKP}}(\gamma,\gamma')/2$ of Eq. (9). By checking the values of those $E_{\mathrm{SKP}}(\gamma,\gamma')$'s which are predicted to be zero by Eqs. (4) and (9), we know how much the superposition assumption [Eq. (4)] is violated.

We use a 64-atom random $\mathrm{Ga}_{0.5}\mathrm{Al}_{0.5}\mathrm{As}$ supercell with unrelaxed atomic positions. This system is large enough to contain many different local Ga and Al arrangements; thus it is useful to test Eq. (4) under these different situations. Supercell LDA potential $V_{\mathrm{LDA}}(\mathbf{r};N_A,N_B)$ and zinc-blende LDA VCA wave functions are used to evaluate $\langle\phi_\gamma^{\mathrm{VCA}}|V|\phi_{\gamma'}^{\mathrm{VCA}}\rangle$. The results are shown in the second column of Table I. In the analytical model [Eq. (9)], the values of the upper half of Table I (case I) are predicted to be zero, either because of $V(\gamma,\gamma')=0$ from Eq. (10), or because of $S(\mathbf{k_0}-\mathbf{k}_0')=0$. In the direct LDA calculation, $\langle\phi_\gamma^{\mathrm{VCA}}|V|\phi_{\gamma'}^{\mathrm{VCA}}\rangle$ is not zero, but it is small: the root-mean-

square (rms) value for the LDA results is 0.11 meV. On the other hand, the values at the lower half of Table I (case II) are not predicted to be zero by symmetry; they have a rms value of 84 meV, about 1000 times larger than the values of case I. So, the violation of the superposition assumption [Eq. (4)] due to the self-consistent potential is very small, only 0.1% as measured by the $\langle \phi_\gamma^{\rm VCA}|V|\phi_{\gamma'}^{\rm VCA}\rangle$ values.

B. Effects of atomic relaxation on superposition assumption

As we see above, the self-consistent LDA potential does not violate Eq. (4) very much. Thus, here we will use the EPM to generate the total potential $V(\mathbf{r};N_A,N_B)$. We calculated an $In_{0.5}Ga_{0.5}As$ 64-atom supercell with the same substitutional configuration as the above $Ga_{0.5}Al_{0.5}As$ system (Ga→In, Al→Ga). We used valence-force-field (VFF) (Ref. 28) method to relax the atomic positions. The fully relaxed atomic positions have average displacements of 0.13 Å for anions, and 0.05 Å for cations. Note that although the total potential can be written as a summation of the atomic screened potentials as in Eq. (13), Eq. (4) which uses unrelaxed ideal position $\mathbf{R}_\mathbf{A}^\mathbf{0}$ [instead of the relaxed position $\mathbf{R}_\mathbf{A}$ as in Eq. (13)] is now not satisfied. As before, $\langle \phi_\gamma^{\rm VCA}|V|\phi_{\gamma'}^{\rm VCA}\rangle$ is calculated using the EPM VCA wave functions $\phi_\gamma^{\rm VCA}$ and $\phi_{\gamma'}^{\rm VCA}$. The results are reported in the fourth column of Table I. As we can see, the rms value in the upper part of Table I (case I) is about 4.3 meV, much larger than the corresponding LDA value without atomic relaxation. But it is still about ten times smaller than the rms value of 44 meV in the lower part of Table I (case II).

C. Error of superposition assumption as a function of the relaxation magnitude

For comparison, the $\langle \phi_\gamma^{\rm VCA}|V|\phi_{\gamma'}^{\rm VCA}\rangle$'s of the unrelaxed $In_{0.5}Ga_{0.5}As$ system are also reported in column 3 of Table I. We see that the values in the lower part of Table I have changed dramaticly after the system was relaxed. It is interesting to know how $\langle \phi_\gamma^{\rm VCA}|V|\phi_{\gamma'}^{\rm VCA}\rangle$'s change as functions of the magnitudes of the relaxations. To achieve different degrees of relaxations, we have changed the VFF parameters as follow:

$$P'_{A(B)}=\tfrac{1}{2}(P_A+P_B)\pm\tfrac{1}{2}\alpha(P_A-P_B), \tag{19}$$

where the $+/-$ sign is for A and B atoms, respectively. Thus, when $\alpha=0$, there is no relaxation, and when $\alpha=1$, there is full relaxation. The resulting $\langle \phi_\gamma^{\rm VCA}|V|\phi_{\gamma'}^{\rm VCA}\rangle$'s as functions of the degree of relaxations α are shown in Fig. 6. From Fig. 6, we found that (i) For the (γ,γ') pairs of case I, the $\langle \phi_\gamma^{\rm VCA}|V|\phi_{\gamma'}^{\rm VCA}\rangle$'s are mainly second-order functions of α. (ii) For the (γ,γ') of case II, the $\langle \phi_\gamma^{\rm VCA}|V|\phi_{\gamma'}^{\rm VCA}\rangle$'s are mainly linear functions of α with fairly large slopes.

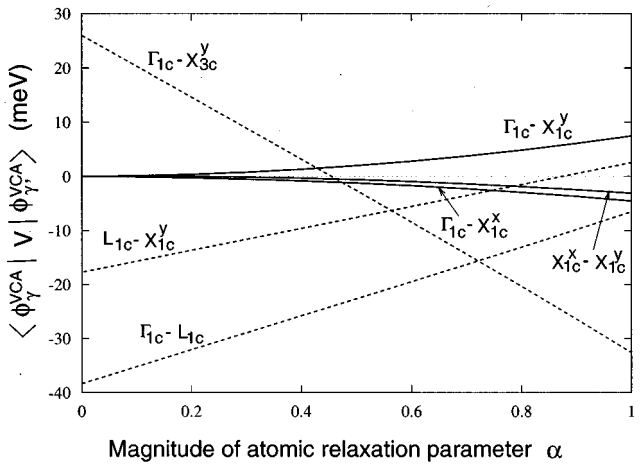

FIG. 6. $\langle \phi_\gamma^{\rm VCA}|V|\phi_{\gamma'}^{\rm VCA}\rangle$'s as functions of the degree of atomic relaxations α [Eq. (19)]. The system is a 64-atom $In_{0.5}Ga_{0.5}As$ alloy supercell as in Table I. The solid lines are predicted to be zero by superposition assumption of Eqs. (4), (9), and (10). They are mainly second-order functions of α.

VII. CONCLUSIONS

In this paper, we have calculated the intervalley couplings for alloys and superlattices. Empirical pseudopotentials are used to construct the total potential [Eq. (13)] and the single-particle Schrodinger's equation [Eq. (12)] is solved for supercells containing up to a few million atoms, using the folded spectrum method[22] and the linear combination of bulk band method.[18] A model [Eqs. (5)–(10)] of the magnitudes of the intervalley coupling is provided based on spectral analysis of the wave functions [Eq. (2)]. The magnitude of the coupling can be divided into a majority contribution term and a minority contribution term [Eq. (5)]. The majority contribution term $2F(\gamma,\gamma')V(\gamma,\gamma')$ is determined by a selection rule on $V(\gamma,\gamma')$ [Eq. (10)] and the magnitude of the overlap function $F(\gamma,\gamma')$ [Eq. (6)]. In general, there are two cases of the intervalley couplings: (i) ''*Strong coupling*,'' where $F(\gamma,\gamma')$ is not small and $V(\gamma,\gamma')$ is not zero, thus the majority contribution is dominant and large. This happens for Γ_{1c}-X_{3c}, Γ_{1c}-L_{1c}, X_{1c}-L_{1c}, X_{1c}-L_{3c}, and X^x_{3c}-X^y_{3c} couplings in cation-mixed alloys. (ii) ''*Weak coupling*,'' where the majority contribution is zero or small, and thus the intervalley coupling comes from the minority contribution (or the majority and the minority contributions have comparable magnitudes). This happens for (a) ''VCA forbidden'' Γ_{1c}-X_{1c}, Γ_{1c}-L_{3c}, X^x_{1c}-X^y_{1c}, and X^x_{1c}-X^y_{3c} couplings in cation-mixed alloys. Here the majority contribution is zero because $V(\gamma,\gamma')=0$, due to the selection rule of Eq. (10). (b) All intervalley couplings in simple superlattices, wires, and dots. Here the majority contribution is small because the small value of $F(\gamma,\gamma')$ due to the localization of the wave functions (regardless whether the coupling states are localized in the same place or in different places).

Regarding the magnitudes and size scalings of the intervalley couplings, we found the following: (1) The strong Γ_{1c}-X_{3c} coupling in a $Ga_{0.5}Al_{0.5}As$ alloy scales as $1/\sqrt{\Omega}$, where Ω is the volume of the system. This scaling and the magnitude of the coupling can be described quantitatively by the majority contribution term (which in this case, equals the single-k-point results). (2) Weak Γ_{1c}-X_{1c} coupling in a $Ga_{0.5}Al_{0.5}As$ alloy is 20–100 times smaller than the Γ_{1c}-X_{3c} coupling. Its majority contribution is zero due to the selection rule of Eq. (10). (3) For the $Ga_{0.7}Al_{0.3}As$ alloy, the CBM has a Γ-point majority representation peak in its spectrum $P_k^{\rm CBM}$, and an L-point minority representation peak, due to

the selection rule of Eq. (10). This minority representation is important in order to obtain the correct bowing coefficients of the alloy eigenstates. (4) In a simple superlattice $(GaAs)_n/(AlAs)_n$, both Γ_{1c}-X_{1c} and Γ_{1c}-X_{3c} couplings are weak coupling, due to the vanishing overlap factor $F(\gamma,\gamma')$ caused by wave-function localization. The coupling magnitudes scale as $1/n^3$. They are 5–100 times smaller than the single-k-point coupling (which describes well the ''strong couplings'' in alloys). This is true for both type-I and -II band alignments in nanostructures. (5) The selection rule of Eq. (10) can be violated in reality due to the fact that real potentials are not describable by the superposition assumption Eq. (4). We find that this leads to a violation by Eq. (10) is 0.1% (measured by the magnitude of $\langle \phi_{\gamma}^{\mathrm{VCA}}|V|\phi_{\gamma'}^{\mathrm{VCA}}\rangle$) due to self-consistency in LDA calculation, and 10% due to an average 0.13 Å atomic relaxation. The magnitude of this violation is roughly a second-order function of the magnitude of the atomic relaxations.

Finally, throughout this paper, we discussed only cation-mixed (or cation-substituted) systems. In the case of anion-mixed system, the same conclusions about the relative amplitudes between different intervalley couplings can be obtained after we exchange the notations of X_{1c} and X_{3c}.

ACKNOWLEDGMENTS

The authors would like to thank Dr. S. H. Wei and Dr. L. Bellaiche for many helpful discussions. This work was supported by the U.S. Department of Energy, OER-BES, under Grant No. DE-AC36-83CH10093.

[1] M. Nakayama *et al.*, Solid State Commun. **88**, 43 (1993).
[2] G. H. Li *et al.*, J. Phys. Chem. Solids **56**, 385 (1995); Phys. Rev. B **50**, 18 420 (1994).
[3] A. Franceschetti and A. Zunger, Phys. Rev. B **52**, 14 664 (1995).
[4] B. Koiller and R. B. Capaz, Phys. Rev. Lett. **74**, 769 (1995).
[5] A. Onton and R. J. Chicotka, Phys. Rev. B **4**, 1847 (1971).
[6] M. H. Meynadier *et al.*, Phys. Rev. Lett. **60**, 1338 (1988).
[7] N. J. Pulsford *et al.*, Phys. Rev. Lett. **63**, 2284 (1989).
[8] S. H. Wei and A. Zunger, Phys. Rev. B **39**, 3279 (1989).
[9] M. Altarelli, Solid State Commun. **15**, 1607 (1974).
[10] L. J. Sham and Y. T. Lu, J. Lumin. **44**, 207 (1989); L. J. Sham, in *The Physics of Low-Dimensional Semiconductor Structures*, edited by P. Butcher *et al.* (Plenum, New York, 1993).
[11] Y. E. Kitaev, A. G. Panfilov, P. Tronc, and R. A. Evarestov, J. Phys.: Condens. Matter **9**, 257 (1997); **9**, 277 (1997).
[12] V. Voliotis *et al.*, Phys. Rev. B **49**, 2576 (1994).
[13] E. L. Ivchenko *et al.*, Solid-State Electron. **37**, 813 (1994).
[14] M. Holtz *et al.*, Phys. Rev. B **41**, 3641 (1990).
[15] M. L. Cohen and J. R. Chelikowsky, *Electronic Structure and Optical Properties of Semiconductors* (Springer-Verlag, Berlin, 1989).
[16] K. A. Mader and Z. Zunger, Phys. Rev. B **50**, 17 393 (1994).
[17] L. W. Wang and A. Zunger, Phys. Rev. B **51**, 17 398 (1995).
[18] L. W. Wang, A. Franceschetti, and A. Zunger, Phys. Rev. Lett. **78**, 2819 (1997).
[19] L. Bellaiche, S. H. Wei, and A. Zunger, Phys. Rev. B **54**, 17 568 (1996).
[20] K. Mader and A. Zunger, Phys. Rev. B **51**, 10 462 (1995).
[21] W. Kohn and L. J. Sham, Phys. Rev. **140**, A1133 (1965).
[22] L. W. Wang and A. Zunger, J. Chem. Phys. **100**, 2394 (1994).
[23] B. Monemar, K. K. Shih, and G. D. Pettit, J. Appl. Phys. **47**, 2604 (1976).
[24] A. L. Efros and M. E. Raikh, in *Optical Properties of Mixed Crystals*, edited by R. J. Elliott and I. P. Ipatova (North-Holland, New York, 1988).
[25] Y. Narukawa *et al.*, Appl. Phys. Lett. **70**, 981 (1997).
[26] H. J. Lee, L. Y. Juravel, J. C. Woolley, and A. J. Spring Thorpe, Phys. Rev. B **21**, 659 (1980).
[27] S. H. Wei and A. Zunger, Phys. Rev. B **52**, 12 039 (1995).
[28] J. L. Martins and A. Zunger, Phys. Rev. B **30**, 6217 (1984).